Performance and Dimensions Determination of an Ejector Utilized in Ejector Cooling Cycle with Eco-Friendly Working Fluids

Sharma, Bharat
National Institute of Technology Kurukshetra

Sachdeva, Gulshan
National Institute of Technology Kurukshetra

https://doi.org/10.5109/7151695

出版情報：Evergreen. 10 (3), pp.1460-1478, 2023-09. 九州大学グリーンテクノロジー研究教育センター
バージョン：

Performance and Dimensions Determination of an Ejector Utilized in Ejector Cooling Cycle with Eco-Friendly Working Fluids

Bharat Sharma[1,*], Gulshan Sachdeva[1]
[1]National Institute of Technology Kurukshetra, India

*Author to whom correspondence should be addressed:
E-mail: bharat_61900103@nitkkr.ac.in

(Received June 13, 2023; Revised August 31, 2023; accepted September 6, 2023).

Abstract: In order to assess the ejector cooling cycle performance and the ejector dimensions, a one-dimensional ejector model is proposed in this paper. The velocity and pressure inside the ejector are examined using thermodynamic governing equations for the eco-friendly working fluids, presuming them as ideal gases. Using conservation of mass, momentum, and energy, the system performance is evaluated. The coefficient of performance (COP) describes the cycle performance, while ejector performance is evaluated in terms of entrainment ratio (ER), mixing area ratio AR_{Mix} and primary nozzle area ratio AR_{Nozzle}. The performance of the cycle is found to improve with the increase in generator and evaporator temperatures, and the decrease in condenser temperature. The area ratios also followed the same trend with the variation of these parameters. At the designed cooling load of 1 kW, the coefficient of performance is found to be 0.182 for R1234ze and 0.061 for R1234yf; and the entrainment ratio of the ejector is 0.237 for R1234ze and 0.08 for R1234yf. As the temperature of the evaporator is increased from 0 to 10℃, the COP is found to rise by 41.41% and 35.56% for R1234ze and R1234yf, respectively. The COP is increased by 6.63% and 40.98% for R1234ze and R1234yf, respectively when the degree of superheat in the generator is enhanced from 2℃ to 6℃ at constant 3000kPa generator pressure.

Keywords: Coefficient of performance, area ratios, entrainment ratio, throat diameters, working fluids-R1234yf, R1234ze.

1. Introduction

As the natural resources are depleting very fast; there is a crucial need to minimize the energy consumption. Refrigeration and air-conditioning systems[1)] consume around 30-40% of total energy consumption during summer in India. The use of low-quality thermal energy to drive these systems for cooling can bring a saving of tons of fuel per year[2)]. Various theoretical and practical applications of solar energy for cooling have been suggested by Sarbu and Sebarchievici[3)]. Ejector cooling cycle (ECC) is the most promising cycle amongst all the non-conventional cooling systems. It has the potential to capture the market due to its reliability, less maintenance requirements, and low preliminary and operational costs. Additionally, the ECC can be helpful to counter the greenhouse effect due to the limited use of electricity and the environmental friendly refrigerants[4,5)]. The ECC requires low-grade thermal energy to produce the cooling effect, and it can operate with a variety of environmental friendly refrigerants. The ECC can work under various operating conditions, however, it is not commercialized due to its low performance (COP) and the imperfect design of ejector geometry[6)]. The performance parameters of the system are entrainment ratio (μ), coefficient of performance (COP), mixing area ratio AR_{Mix} and primary nozzle area ratio AR_{Nozzle}. Mixing area ratio AR_{Mix} is defined as the ratio of area of the mixing section (A_{Mix}) to the area at the throat of primary nozzle (A_{Th}) whereas, the nozzle area ratio AR_{Nozzle} is defined as the ratio of area at the throat of primary nozzle (A_{Th}) to the area at the exit of primary nozzle (A_{NExit}). To improve the performance of the ECC, many experimental and theoretical analysis have been done at different operating conditions. To calculate the ejector performance, Keenan et al.[7)] projected an analytical model based on the constant pressure mixing theory of ejector. Munday and Bagster[8)] introduced the concept of double choking phenomena for a fixed-geometry ejector. They explained that primary fluid runs out from the nozzle without mixing with the entrained (secondary) fluid. The primary fluid contined to expand in the constsnt area section and formed a convergent section for the secondary fluid. Huang et al.[9)] analysed a 1-D ejector model based on constant-pressure mixing theory, however, the mixing was assumed to start at the

hypothetical throat area formed in the constant area section. Purjam et at.[10] simulated the ECC by adding a turbo-expander in between the ejector and evaporator. The ejector dimensions and operating conditions have the greatest influence on the behavior of the ejector as well as the system performance. The dimensions of the ejector geometry had been investigated using thermodynamic models [11], or conducting experimentals[12] as well as employing computational fluids dynamics models[13]. Many researchers have further carried out the energy[14,15] exergy[16–18] analysis of the ejector cooling system.

Ejector geometry is a very critical parameter that affects the systems performance. The "grey relation analysis", a mathematical model given by He et al.[19] described the effect of Nozzle Area Ratio and Nozzle Exit Positon (NXP) on the performance of the ejector. The primary nozzle exit position (NXP) is the distance of constant area section from the primary nozzle exit and it is considered zero at the inlet of the constant area section (CAS). It is considered positive if it is inside the CAS and negative if it is towards the primary nozzle. Nguyen et al.[20] investiaged the effect of nozzle exit position of a solar ejector refrigeration system. The NXP had been varied from 3 to 7mm. The system performance was found to increase till 5mm NXP and then got decreased. The authors also concluded that the performance is very sensitive to the area ratio than the NXP. The effect of varying the convergent angle of the mixing section was analysed by Zhu et al.[21] using CFD tools. They concluded that changing the convergent angle (θ) of the mixing section from 0º to 26.56º varried the entrainment ratio (μ) up to 16.9%. The maximum entrainment ratio was achieved at 1.45º convergent angle. Yan et al.[22] also worked on similar parameters using CFD for R134a refrigerant. The maximum improvement in ejector performance was obtained by varying the convergent angle in comparison to the divergent angle and NXP. The improvement in ejector entrainment ratio was found to be 41.2% at 8.5°C evaporating temperature. Haghparast et. al. [23] performed experiments to analyse the effect of nozzle exit diameter on the ejector efficiency, and found the increase in ejector efficiency by 21% by varying the nozzle exit diameter from 18mm to 23mm. An experimental model of steam ejector was developed by Eames et al.[24] to analyze the geometry parameters. Yapici et al.[25] experimented using refrigerant R123, and found that increasing the generator temperature linearly increases the nozzle area ratio and the optimum NXP lies between -10 to 5mm for minimum suction pressure. Rusly E[13] concluded that by increasing the nozzle area ratio, the shock generated in the constant area section (CAS) got shifted inside the CAS which resulted in decreasing the critical backpressure. Moreover, they determined the area ratio that satisfies the requirement of double choking condition for the optimum performance of the ejector. Jia et al.[26] executed a 1-D analysis on an air-cooled refrigeration cycle using R134a and varied the area ratio linearly from 3.69-4.76 and the generator pressure from 20.5 to 25 bar. A few researchers have also expressed the effect of the ratio of length to the diameter of the different sections of the ejector after conducting experiments. Varga et. al.[27] studied the effects of varying the length of the mixing and the constant area section in terms of the shock wave location in the ejector. Chong et al.[28] affirmed that critical back-pressure was found to increase as the ratio of mixing section length and its diameter were increased. Wu et al.[29] concluded that the entrainment ratio got increased linearly with the increase in the mixing length of the steam ejector cycle. Banasiak et al.[30] suggested the optimum length of the mixing section between 20-25 mm while working experimentaly and numerically with R744.

The inference of the literaturestudy are: (1) constant-pressure mixing theory is highly effective than constant-area mixing theory; (2) fixed ejector geometry has fixed back pressure that limits the mass flow rate of working fluid; (3) ejector and system performance mainly depend on the properties of working fluids, operating parameter, and ejector design; (4) operating conditions of the ECC must be predefined. (5) above deductions mainly agree with fixed ejector geometry.

The working fluid also strongly influences the cycle performance and the ejector function. It has now become important to give equal consideration to the environmental aspects like ozone depletion potential (ODP), global warming potential (GWP), and atmospheric lifetime (ALT), toxicity, auto ignition and supply considerations of the refrigerants. Therfore, two eco friendly refrigerants i.e. R1234yf, and R1234ze have been chosen in the present study and their performance has been compared with the most widely used refrigerant R134a which is going to be phased out soon. The novelty of the work lies in analyzing two new eco-friendly refrigerants and determination of the dimensions of the ejector employed in the ejector cooling system.

2. Cycle description and assumptions

The ejector cooling cycle is a heat-assisted cooling system that involves an ejector, a pump, a throttling valve and three heat exchangers i.e. generator, condenser, and evaporator as shown in figure 1-a. The corresponding T-s diagram is shown in figure 1-b. Ejector works as a substitute to the compressor with two inflows and one outflow. High-pressure saturated vapor stream, called primary stream, from the generator inflows into the primary nozzle, expands and creates low pressure in the ejector. It causes a low pressure saturated vapor stream called secondary stream, from the evaporator to inflow in the ejector. Both the streams get mixed at constant pressure in the mixing area section and the diffuser increases the pressure to the condenser presssure before the mixed stream outflows from the ejector. The condenser dissipates its heat. The condensed saturated liquid stream is split. One portion is expanded in the expansion valve and then take cooling load in the

evaporator. The other portion is pumped to the generator wherein it takes heat and transforms into saturated vapor. This way the cycle continues.

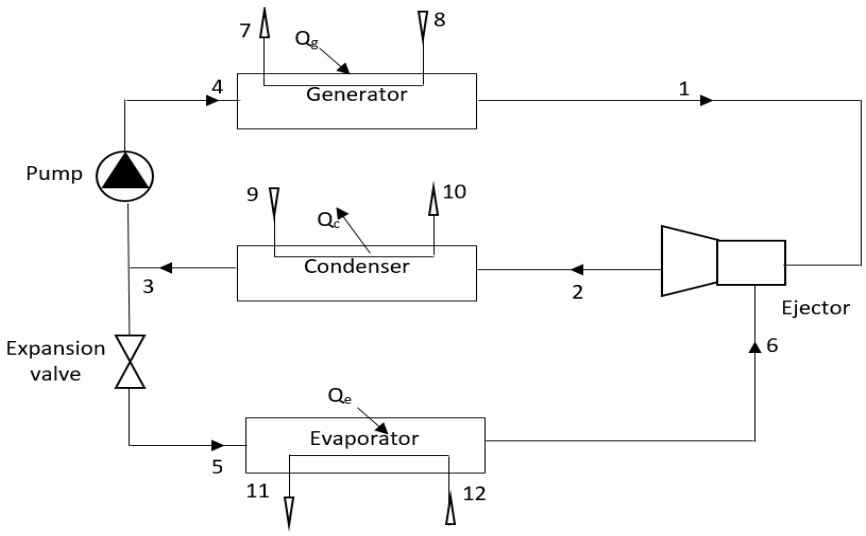

Fig. 1-a: Ejector Cooling Cycle

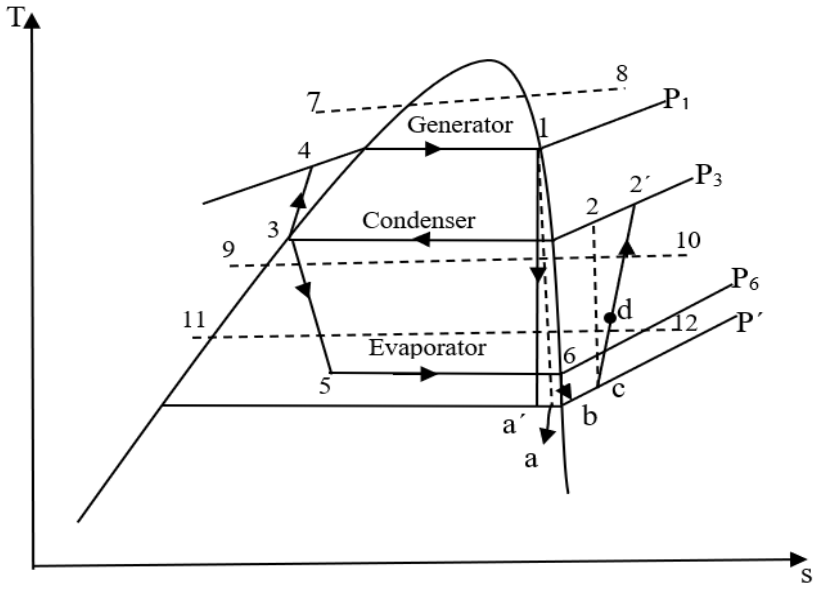

Fig. 1-b: T-s illustration of the ECC

The following assumptions have been made while analyzing the system:

I. The flow is uniform and one-dimensional in all the sections of ejector.
II. The working fluid is assumed to behave like an ideal gas in the ejector.
III. Pressure and heat loss in the ejector and system are considered negligible.
IV. The primary and the secondary fluids are saturated and their velocities at the ejector inlets are negligible.
V. The system is designed for a fixed cooling capacity of 1.0 kW.
VI. All losses in the ejector are considered in terms of the efficiencies of the nozzle, mixing and diffuser. These are considered constant and same as 90% i.e. $\eta_n = \eta_m = \eta_d = 90\%$. The efficiency of the pump is supposed to be 80% i.e. $\eta_p = 80\%$.
VII. Water is used as the external fluid in the heat exchangers.
VIII. Mixing of primary and secondary vapor takes place in the suction section at a constant pressure.
IX. The primary and secondary vapor have the same molecular weight and specific heat ratio.

3. Mathematical Modelling

A mathematical model is prepared in the current communication wherein the equations are similar to those used by Chen et al[31]. The cycle is simulated using Engineering Equation Solver EES[32] as it has an inbuilt library of the properties of the refrigerants used in the analysis.

3.1 Governing equations:

The governing equations for the components of ECC are based on mass, momentum, and energy conservation and are mentioned as under. The subscripts used in these equations are according to the figure 1-b.

3.1.1 Primary fluid expansion (1-a):

The primary flow expands in the nozzle and the velocity (V_a) at its exit is given by:

$$V_a = \sqrt{2(h_1 - h_a)} \quad (1)$$

where h_1 and h_a are the specific enthalpies of the primary flow at entry and exit.

To consider various losses in the nozzle, the isentropic efficiency of the nozzle (η_n) is considered as below:

$$\eta_n = \frac{h_1 - h_{a'}}{h_1 - h_a} \quad (2)$$

The specific enthalpy $h_{a'}$ is the function of assumed mixing pressure, which is iterated to find the correct value, and isentropic expansion of primary flow.

Using equations (2) and (1), the actual exit velocity is determined as:

$$V_a = \sqrt{2\eta_n(h_1 - h_{a'})} \quad (3)$$

Assuming ideal gas behavior, the expansion of primary flow is expressed in terms of Mach number (M_{1a}) at the exit of the nozzle[33,34] as under:

$$M_a = \sqrt{\frac{2\eta_n}{\gamma - 1}\left[\left(\frac{P_1}{P'}\right)^{\left(\frac{\gamma-1}{\gamma}\right)} - 1\right]} \quad (4)$$

P' is the mixing pressure of the ejector.

3.1.2 Secondary fluid entrainment (6-b):

In the previous studies[33,35], the velocity of the secondary flow had been neglected assuming that both the fluids got mixed at the evaporator pressure. However, It is not a reasonable assumption as the refrigerant pressure exiting from the evaporator drops down to the mixing pressure. Considering the fact and using conservation of energy, the secondary flow velocity (V_b) is expressed as under:

$$V_b = \sqrt{2(h_6 - h_b)} \quad (5)$$

where h_b is the function of mixing pressure and secondary flow exit entropy. It is expressed as under

$$h_b = f(P', s_6) \quad (6)$$

The Mach number of the secondary flow at state point b[12] is expressed as under:

$$M_b = \sqrt{\frac{2}{\gamma - 1}\left[\left(\frac{P_6}{P'}\right)^{\left(\frac{\gamma-1}{\gamma}\right)} - 1\right]} \quad (7)$$

3.1.3 Mixing of the fluids before the shock

The primary and secondary fluid get mixed in the mixing section before the shock formation takes place at point 'd'. The conservation of mass and momentum balance of this ideal mixing happens at the constant mixing pressure:

$$\dot{m}_2 = \dot{m}_1 + \dot{m}_6 \quad (8)$$

where $\dot{m}_2, \dot{m}_1 \; and \; \dot{m}_6$ are the mass flow rate at the mentioned state points.

$$\dot{m}_2 V_2 = \dot{m}_1 V_a + \dot{m}_6 V_c \quad (9)$$

where V in the above equation is the velocity at the state poined mentioned.

The ideal velocity of the mixed flow using equations (8) and (9) is expressed as:

$$V_{c'} = \frac{V_1 + \mu' V_6}{1 + \mu'} \quad (10)$$

where μ′ is an assumed entrainment ratio of the ejector, defined as ratio of the secondary mass flow rate to the primary mass flow rate and it is expressed as under:

$$\mu' = \frac{\dot{m}_6}{\dot{m}_1} \quad (11)$$

The mixing efficiency (η_m) is the ratio of actual velocity to the ideal velocity of the mixed flow before shock formation and is found as under:

$$\eta_m = \frac{V_c^2}{V_{c'}^2} \quad (12)$$

The actual velocity (V_c) for the mixed flow using equations 10 and 12 is expressed as:

$$V_c = \sqrt{\eta_m}\frac{V_a + \mu' b}{1 + \mu'} \quad (13)$$

The actual specific enthalpy (h_c) of the mixed flow can be found applying the conservation of energy. It is expressed as under:

$$\dot{m}_1 h_1 + \dot{m}_6 h_6 = \dot{m}_c h_c + \frac{V_c^2}{2} \quad (14)$$

After modifying the primary and secondary mass flow rate in terms of entrainment ratio (μ), the actual specific enthalpy is expressed as [35]:

$$h_c = \frac{h_1 + \mu' h_6}{1 + \mu'} - \frac{V_c^2}{2} \quad (15)$$

The actual entropy at state c i.e. s_c can be obtained using $P'$and h_c. In a functional form, it is expressed as[35]:

$$s_c = f(P', h_c) \quad (16)$$

Combining the aforementioned equations while taking into account mixing efficiency (η_m) yield the critical

Mach number at state c (M_c^*) in terms of the critical Mach numbers of the primary flow (M_{1a}^*) and the secondary flow (M_{6b}^*) at state 'a'.

$$M_c^* = \sqrt{\eta}_m \frac{\left(M_a^* + \mu' M_b^* \sqrt{\frac{T_6}{T_1}}\right)}{\sqrt{(1+\mu')*\left(1+\mu'\frac{T_6}{T_1}\right)}} \quad (17)$$

where T_6 *and* T_1 are the temperatures of evaporator and generator respectively.

At any location inside the ejector, the relation between the Mach number and the critical Mach number can be written as[36]:

$$M^* = \sqrt{\frac{M^*(\gamma+1)}{M^*(\gamma+1)+2}} \quad (18)$$

Equation (17) allows for the calculation of the Mach number of the mixed flow at state c (M_c) from M* (17) and it is expressed as:

$$M_c = \sqrt{\frac{2M_c^{*2}}{(\gamma+1)-2M_c^{*2}(\gamma+1)}} \quad (19)$$

The velocity of the mixed flow changes from supersonic to a subsonic flow and a shock generates that produces a sudden pressure rise when $M_c > 1$.

3.1.4 Expansion in the diffuser (c-2):

Neglecting velocity at the exit of the diffuser, the specific enthalpy (h_2) is expressed as under:

$$h_2 = h_c + \frac{V_c^2}{2} \quad (20)$$

Diffuser efficiency (η_d) is defined as the ratio of isentropic enthalpy difference to the actual enthalpy difference due to expansion. It is expressed as:

$$\eta_d = \frac{h_{2\prime} - h_c}{h_2 - h_c} \quad (21)$$

The actual specific enthalpy (h_2) can also be expressed in terms of diffuser efficiency as under:

$$h_2 = h_c + \frac{h_{2\prime} - h_c}{\eta_d} \quad (22)$$

The actual entrainment ratio (μ)[36] of the ejector can be expressed using the above equations as:

$$\mu = \frac{\sqrt{2\eta_n(h_1 - h_{a\prime})} - \sqrt{\frac{2\left(h_{2\prime} - h_c\right)}{\eta_d \eta_m}}}{\sqrt{\frac{2\left(h_{2\prime} - h_c\right)}{\eta_d \eta_m}} - \sqrt{2(h_6 - h_b)}} \quad (23)$$

The shock is generated in the constant area section (c-d), due to which the pressure is increased. The Mach number after shock (d) and the pressure are expressed as [37]:

$$M_d = \sqrt{\frac{M_c^2 + 2/(\gamma+1)}{\frac{2M_c^2}{(\gamma+1)} + 1}} \quad (24)$$

$$\frac{P_d}{P_c} = \frac{1+\gamma M_c^2}{1+\gamma M_d^2} \quad (25)$$

Pressure recovery in the diffuser can be expressed as[37]:

$$\frac{P'_2}{P_d} = \left[1 + \frac{\eta_d(\gamma-1)}{2} M_2^2\right]^{\frac{\gamma}{(\gamma-1)}} \quad (26)$$

The diffuser exit pressure P'_2 is isentropic pressure calculated using equation 26 and iterated comparing with the condenser pressure P_2. Therefore, two iterations are used to determine the entrainment ratio (μ) and diffuser exit pressure (P_2).

3.1.5 Ejector geometry and system performance:

The ejector geometry is specified by area at the throat of primary nozzle A_{Th}, mixing area ratio AR_{Mix} and primary nozzle area ratio AR_{Nozzle}. Mixing area ratio AR_{Mix} is defined as the ratio of area of the mixing section (A_{Mix}) to the area at the throat of primary nozzle (A_{Th}) whereas, the primary nozzle area ratio AR_{Nozzle} is defined as the ratio of area at the throat of primary nozzle (A_{Th}) to the area at the exit of primary nozzle (A_{NExit}). The equations used for the determination of these parameters are mentioned as under-

$$A_{Th} = \frac{\dot{m}_1}{P_1}\sqrt{\frac{RT_1}{\gamma\eta_n}}\left(\frac{\gamma+1}{2}\right)^{\left(\frac{\gamma+1}{\gamma-1}\right)} \quad (27)$$

$$AR_{Mix} = \frac{P_1\sqrt{(1+\mu)*\left(1+\mu\frac{T_6}{T_1}\right)}*\left(\frac{2}{\gamma+1}\right)^{\frac{1}{\gamma-1}}*\sqrt{1-\frac{2}{(\gamma+1)}}}{P_2\left(\frac{P_e}{P_2}\right)^{\frac{1}{\gamma}}*\sqrt{1-\left(\frac{P_e}{P_2}\right)^{\frac{\gamma-1}{\gamma}}}} \quad (28)$$

$$AR_{Nozzle} = \frac{1}{M_{1a}^2}\left(\frac{2}{\gamma+1}\left(1+\frac{\gamma+1}{2}M_{1a}^2\right)\right)^{\frac{\gamma+1}{\gamma-1}} \quad (29)$$

The heat interaction in the heat exchangers is calculated using energy.

$$Q_{Gen} = \dot{m}_1(h_1 - h_4) \quad (30)$$

$$Q_{Con} = \dot{m}_2(h_2 - h_3) \quad (31)$$

$$Q_{Eva} = \dot{m}_6(h_6 - h_5) \quad (32)$$

Work done by the pump is calculated as under-

$$W_{Pump} = \dot{m}_1(h_4 - h_3) \quad (33)$$

The coefficient of performance (COP) of the ECC is the ratio of the cooling effect produced in the evaporator to the generator heat and pump work.

$$COP = \frac{Q_{Eva}}{Q_{Gen}+W_{Pump}} = \frac{\dot{m}_6(h_6-h_5)}{\dot{m}_1(h_1-h_3)} = \mu\frac{(h_6-h_5)}{(h_1-h_3)} \quad (34)$$

3.2 Computational procedure

To determine the cycle performance and the ejector geometry, a computational procedure has been followed. It iterates the assumed variables, entrainment ratio (μ) and mixing pressure (P′), to their technically correct values. The procedure is explained in figure 2.

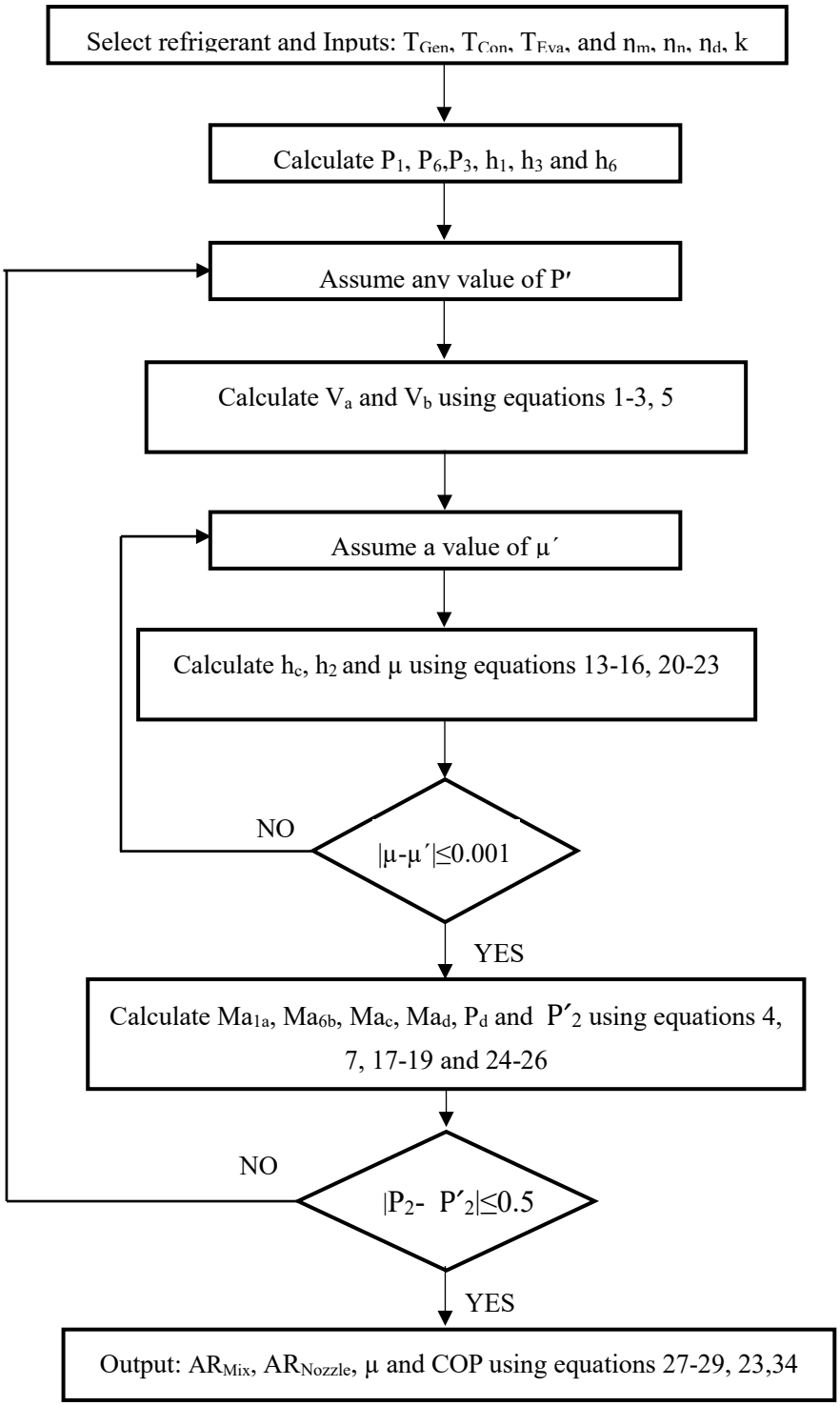

Fig. 2: Flow chart of ECC

3.3 Model Validation

The performance and geometry parameters i.e. COP, Nozzle Area Ratio and Entrainment Ratio obtained for the refrigerant R134a are validated at the same input conditions as provided by Saleh B[38]. Table 1 shows that the variation of these parameters with respect to generator temperature are in coherence with the work[38].

Table 1. Validation with Saleh B.[38]

	Saleh B.[38]			**Current Model**		
T_{Gen} (°C)	COP	μ	AR_{Nozzle}	COP	μ	AR_{Nozzle}
70	0.06	0.073	2.96	0.075	0.083	2.44
75	0.109	0.126	3.39	0.115	0.13	3.89
80	0.15	0.173	3.87	0.159	0.185	4.24
85	0.185	0.213	4.39	0.189	0.213	4.79

90	0.215	0.243	4.95	0.214	0.239	5.02
95	0.235	0.259	5.56	0.227	0.266	6.02
100	0.239	0.301	6.57	0.243	0.293	6.59

4. Results and discussion:

In this section, the influence of different working fluids on ejector cooling cycle (ECC) performance and dimensions like area ratios and various diameters of the ejector with different cooling capacities have been studied for the refrigerants R134a, R1234yf, and R1234ze at different evaporator temperatures, condenser temperatures, and generator pressures. The ejector cooling system is designed for 10°C evaporator, 40°C condenser temperature and 3000kPa generator pressure with 2 degrees of superheat and 1.0 kW cooling capacity. The assumed efficiencies of ejector components are 90%. The thermodynamics equations are written in Engineering Equation Solver (EES)[32] and the results are achieved using inbuilt properties of the refrigerants in EES.

4.1 Effect of evaporator temperature

4.1.1 On the system performance

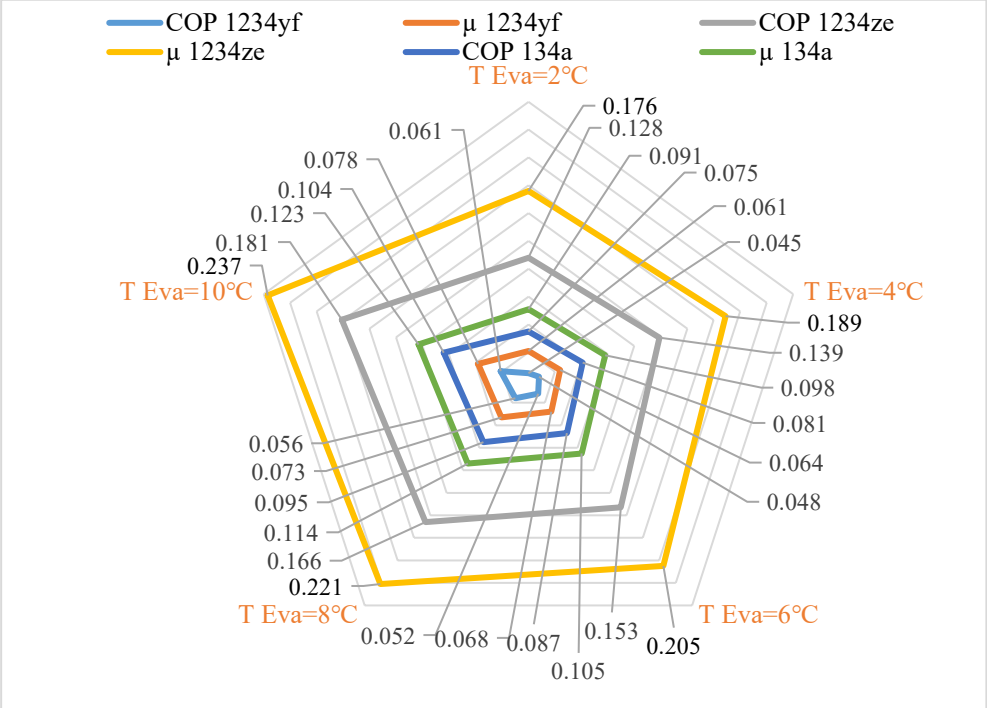

Fig. 3: Influence of evaporator temperature on COP and μ

Figure 3 depicts that the decrease in evaporator temperature from 10°C to 2°C decreases COP and μ for all the working fluids. The COP of the system is decreased by 26.23%, 29.28% and 27.88% for R1234yf, R124ze and R134a respectively. Figure 3 shows that R1234ze has the highest COP and R1234yf has the lowest COP at any evaporator temperature. The entrainment ratio (μ) also varies in the same decreasing trend with the decrease of evaporator temperature from 10°C to 2°C for all the working fluid. The entrainment ratio is decreased by 21.79%, 25.74% , and 26.02% for R1234yf, R124ze and R134a respectively. Figure 3 also shows that R1234ze has the highest entrainment ratio among the refrigerants considered in the study. Figure 4 reveals the influence of evaporator temperature on the mixing pressure (P′) of primary and secondary fluids. Figure 4 shows that this pressure lies below the evaporator temperature for all the working fluids. The mixing pressure (P′) is found to decrease with the decrease in evaporator temperature by 1.94% in case R1234ze working fluid and 0.91% for R134a. The influence of evaporator temperature on mixing area ratio and nozzle area ratio is shown in table 2. The mixing area ratio is found to increase a little with the increase in evaporator temperature but the nozzle area ratio is decreased for the same operating conditions. The mixing area ratio is increased by 1.18% for R1234yf, 3.17% for R1234ze and 1.42% for R134a and and the nozzle area ratio is decreased by 0.24% for R1234yf, 1.12% for R1234ze and 0.56% for R134a for R1234ze respectively.

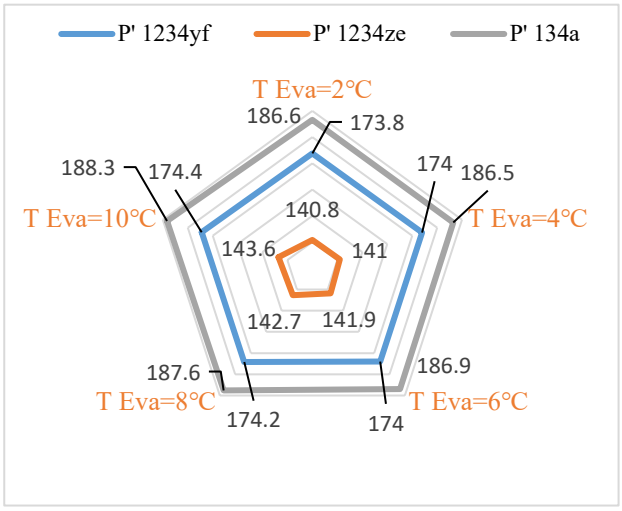

Fig. 4: Mixing pressure Influence by the variation of evaporator temperature

Table 2: Influence of evaporator temperature on area ratio with different working fluids.

T_{Eva}	R1234yf		R1234ze		R134a	
(°C)	AR_{Mix}	AR_{Nozzle}	AR_{Mix}	AR_{Nozzle}	AR_{Mix}	AR_{Nozzle}
2	3.72	3.72	5.14	4.19	3.75	3.57
4	3.73	3.71	5.17	4.18	3.73	3.57
6	3.74	3.71	5.21	4.17	3.76	3.57
8	3.76	3.71	5.25	4.16	3.78	3.56
10	3.77	3.71	5.30	4.14	3.80	3.55

4.1.2 On the ejector dimension

The dimensions of the ejector also get affected by the variation of evaporator temperature. Figure 5(a) shows that the throat diameter is increased when the evaporator temperature is decreased. The throat diameter is found to increase by 15.89%, 18.72%, and 17.87% for R1234yf, R1234ze, and R134a respectively. The maximum throat diameter is 9.77 mm for R1234yf at the evaporator temperature of 2°C, and the minimum diameter is 8.43mm for R1234ze fluid at 10°C evaporator temperature. The decrease in evaporator temperature increases the primary mass flow rate and hence improves the system performance. The effect is similar on the nozzle exit diameter with the change in evaporator temperature. Figure 5(b) reveals that the nozzle exit diameter is increased by 15.89%, 19.37%, and 18.15% for R1234yf, R1234ze, and R134a for the change in evaporator temperature from 10°C to 2°C. The maximum nozzle exit diameter is 11.03 mm at 2°C and minimum nozzle exit diameter is 9.24mm at 10°C for R1234ze. The effect of evaporator temperature on the constant area diameter also followed the same trend as the other diameters. Figure 5(c) shows that the constant area diameter is increased with the decrease of evaporator temperature by 15.22%, 10.46%, and 16.78% for R1234yf, R1234ze, and R134a respectively. The constant-area diameter is always highest for R1234yf and lowest for R1234ze for the range of evaporator temperatures considered.

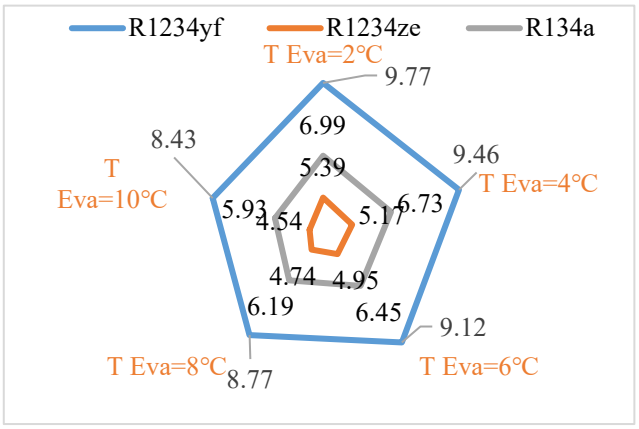

(a) Throat Diameter (mm)

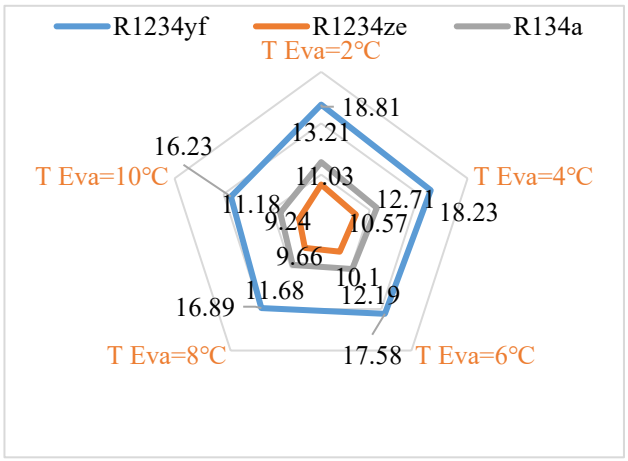

(b) Nozzle exit diameter (mm)

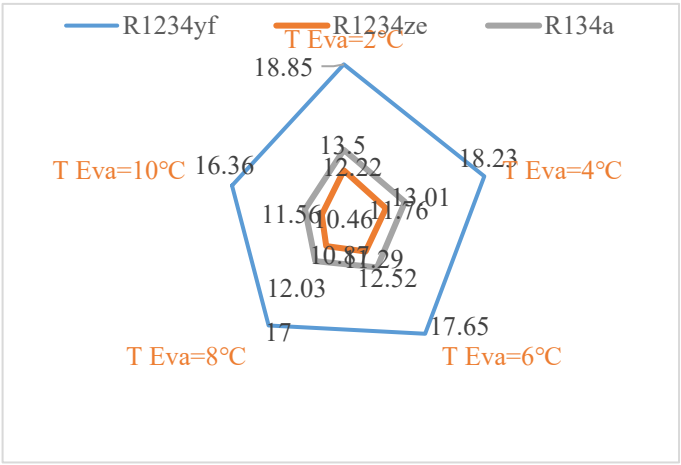

(c) Constant area diameter (mm)

Fig. 5: Influence of evaporator temperature on ejector dimensions

4.1.3 On refrigerant mass flow rate and heat load

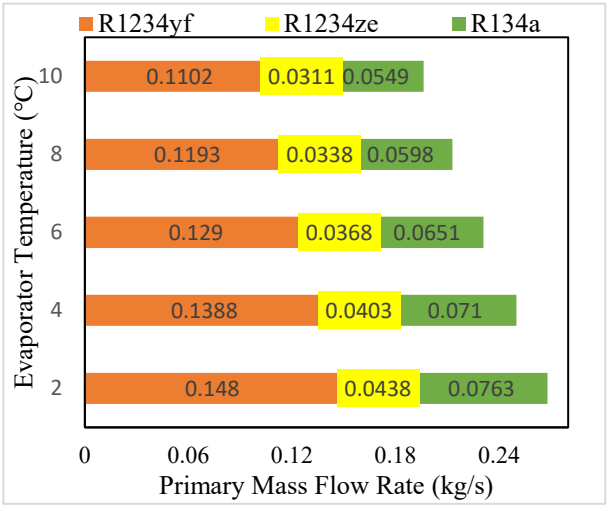

(a) Primary mass flow rate

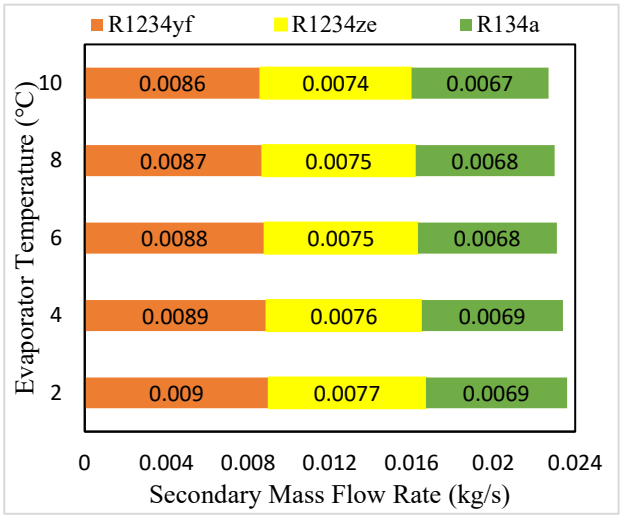

(b) Secondary mass flow rate

Fig. 6: Influence of evaporator temperature on mass flow rate.

Figure 6 (a) and (b) show that both primary and secondary mass flow rates are increased with the decrease in evaporator temperature from 10°C to 2°C and the rate of decrease of primary mass flow is more than that of secondary fluid. The primary fluid flow rate is increased by 40.83%, 34.30% and 38.98% for R1234ze, R1234yf and R134a respectively when the evaporator temperature is varied from 10°C to 2°C . The secondary mass flow rate is found to increase by 4.65%, 4.05%, and 2.98% for R1234ze, R1234yf and R134a respectively.

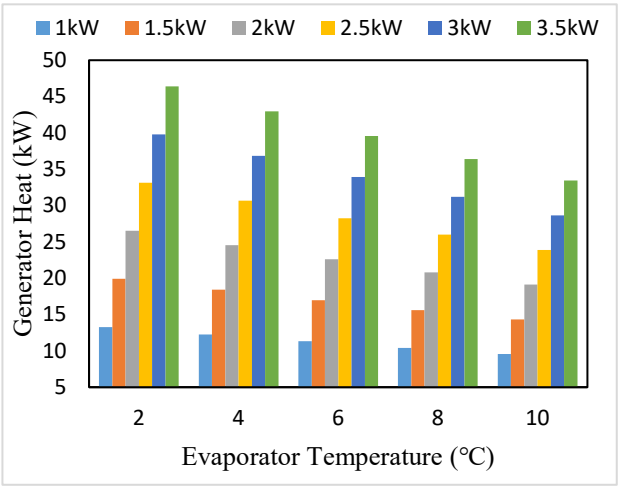

(a) Generator heat load (kW)

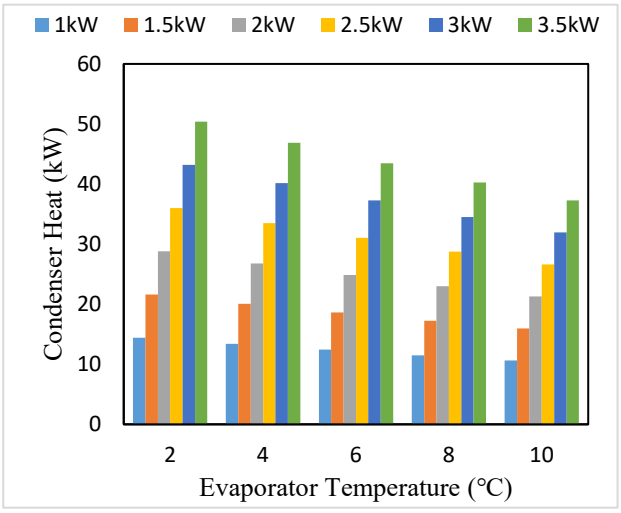

(b) Condenser heat load (kW)

Fig. 7: Influence of evaporator temperature on heat load for R134a.

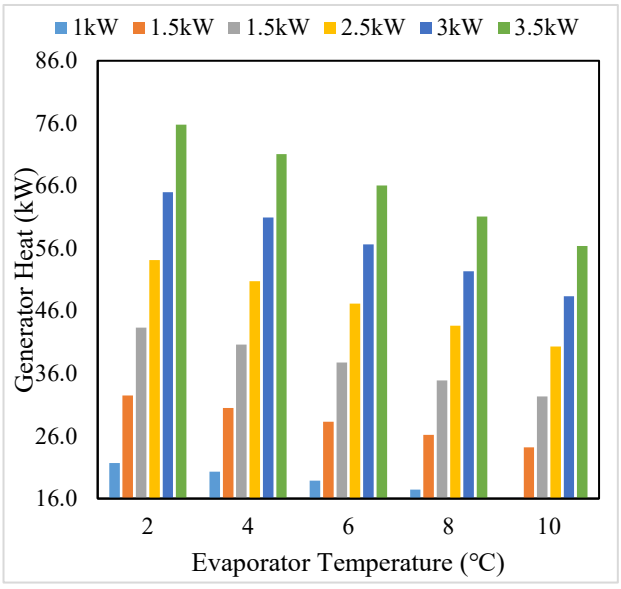

(a) Generator heat load (kW)

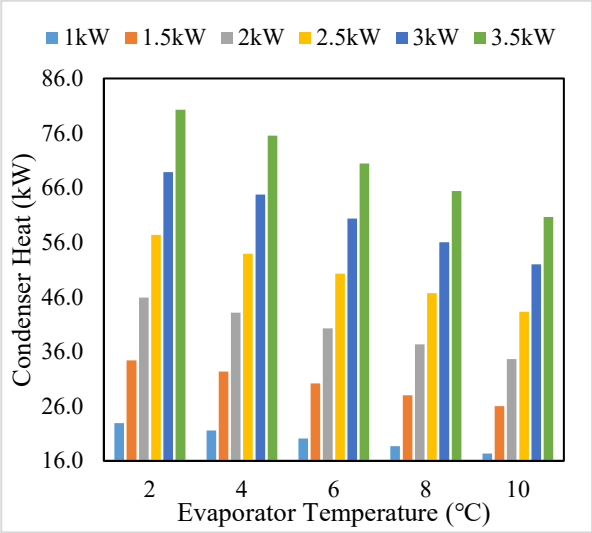

(b) Condenser heat load (kW)

Fig. 8: Influence of evaporator temperature on heat load for R1234yf.

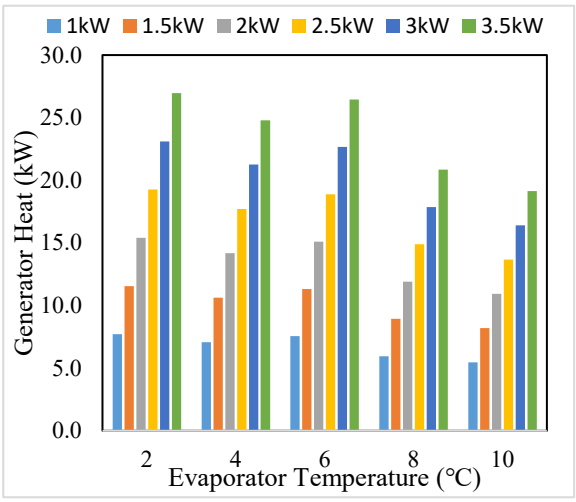

(a) Generator heat load (kW)

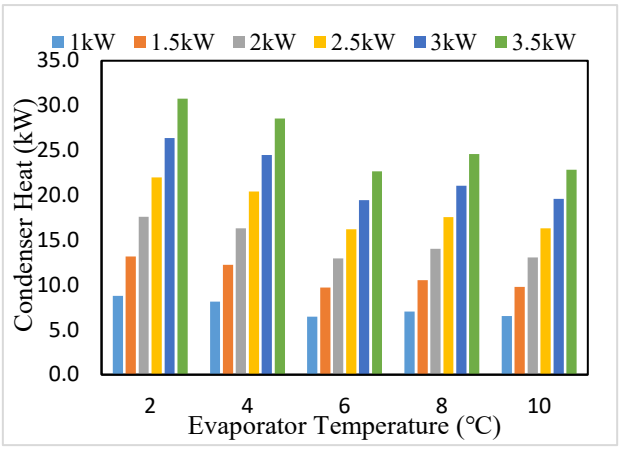

(b) Condenser heat load (kW)

Fig. 9: Influence of evaporator temperature on heat load for R1234ze.

Figures 7 (a) and (b) show the effects of evaporator temperature on the change of heat load in the generator and the condenser for the refrigerant R134a. Similarly figures 8 and 9 show variations of the same variables for the refrigerants R1234yf and R1234ze respectively. It can be seen from the respective figures that the heat load in both the generator and condenser is increased with the decrease in evaporator temperature from 10°C to 2°C for the working fluid. The heat load in the generator and condenser are increased by 34.36% and 32.37% respectively when the evaporator temperature is decreased from 10°C to 2°C while operating at 1 kW cooling capacity with R1234yf. The heat content required in the generator is found to increase by 250% when the refrigeration capacity is increased from 1 kW to 3.5 kW. Observations are similar with R134a and R1234ze.

4.2 Effect of condenser temperature

4.2.1 On the system performance

Figure 10 depicts that the increase in condenser temperature from 32°C to 40°C decreases COP and μ for all the working fluids. The COP of the system is decreased by 71.63%, 50.27% and 61.62% for R1234yf, R124ze and R134a respectively. It also shows that R1234yf has the highest COP and R1234ze has the lowest COP at any condenser temperature. The entrainment ratio (μ) is also found ot decrease with the increase of condenser temperature from 32°C to 40°C for all the working fluids. The entrainment ratio is decreased by 71.01%, 49.49% , and 61.19% for R1234yf, R124ze and R134a respectively. Figure 10 also shows that R1234ze has the highest entrainment ratio among the refriegrants considered in the study. Figure 11 reveals that the mixing pressure (P′) is increased with the increase in condneser temperature by 7.92% in case R1234yf, 9.62% for R1234ze working fluid and 11.88% for R134a. The influence of condenser temperature on mixing area ratio and nozzle are ratio are shown in table 3. The mixing area ratio and the nozzle area ratio are found to decrease with the increase in condenser temperature for the same operating conditions. The mixing area ratio is decreased by 23.92% and 25.35% and the nozzle area ratio is decreased by 4.24% and 5.15% for R1234yf and R1234ze respectively. The mixing pressure is always lower for R1234ze fluid followed by R1234yf and R134a because R1234ze has high critical pressure used for others.

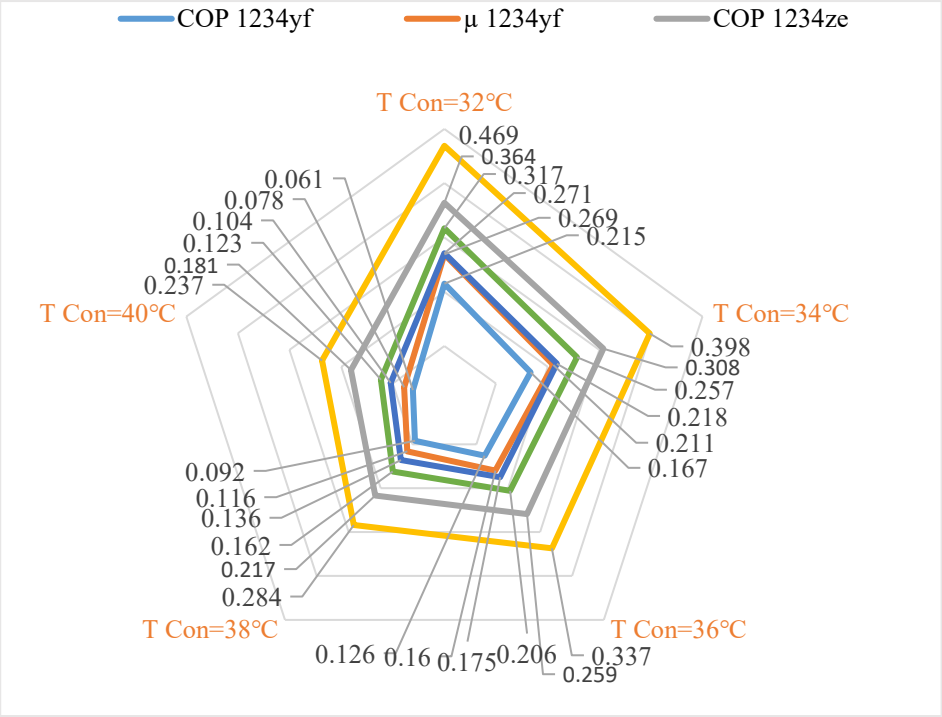

Fig. 10: Influence of condenser temperature on COP and μ

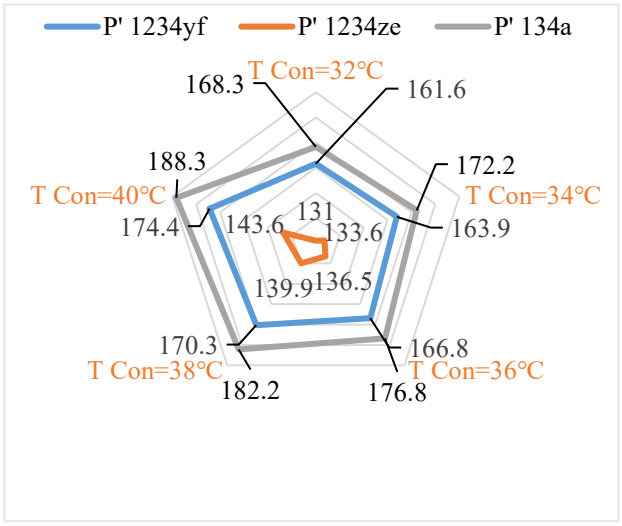

Fig. 11: Mixing pressure Influence by the variation of the variation of condenser temperature

Table 3: Influence of condenser temperature on area ratio with different working fluids.

T_{Eva}	R1234yf		R1234ze		R134a	
(°C)	AR_{Mix}	AR_{Nozzle}	AR_{Mix}	AR_{Nozzle}	AR_{Mix}	AR_{Nozzle}
32	4.95	3.87	7.10	4.36	5.07	3.78
34	4.61	3.84	6.57	4.32	4.70	3.73
36	4.30	3.80	6.10	4.26	4.37	3.68
38	4.02	3.76	5.68	4.20	4.07	3.62
40	3.77	3.71	5.30	4.14	3.80	3.55

4.2.2 On the ejector dimensions

Figure 12(a) shows that the throat diameter is increased when the condenser temperature is increased. The throat diameter is found to increase by 94.68%, 46.45%, and 67.04% for R1234yf, R1234ze, and R134a respectively. The maximum throat diameter is 8.43mm for R1234yf at the condenser temperature of 40°C, and the minimum diameter is 3.1mm for R1234ze fluid at 32°C condenser temperature. The effect is similar on the nozzle exit diameter with the change in condnenser temperature. Figure 12(b) reveals that the nozzle exit diameter is increased by 47.44%, 29.87%, and 38.19% for R1234yf, R1234ze, and R134a for the change in condenser temperature from 32°C to 40°C. The maximum nozzle exit diameter is 9.24 mm at 40°C and minimum nozzle exit diameter is 6.48mm at 32°C for R1234ze. The effect of condenser temperature on the constant area diameter also followed the same trend as the other diameters. Figure 12(c) shows that the constant area diameter is increased with the increase of condenser temperature by 41.07%, 21.03%, and 30.79% for R1234yf, R1234ze, and R134a respectively. The constant-area diameter is always highest for R1234yf and lowest for R1234ze for the range of condenser temperatures considered.

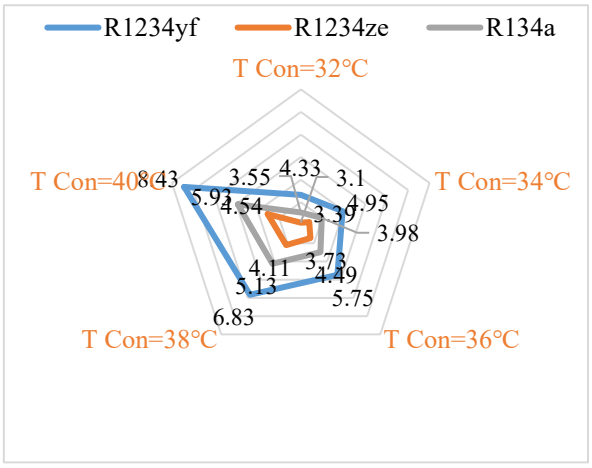

(a) Throat diameter (mm)

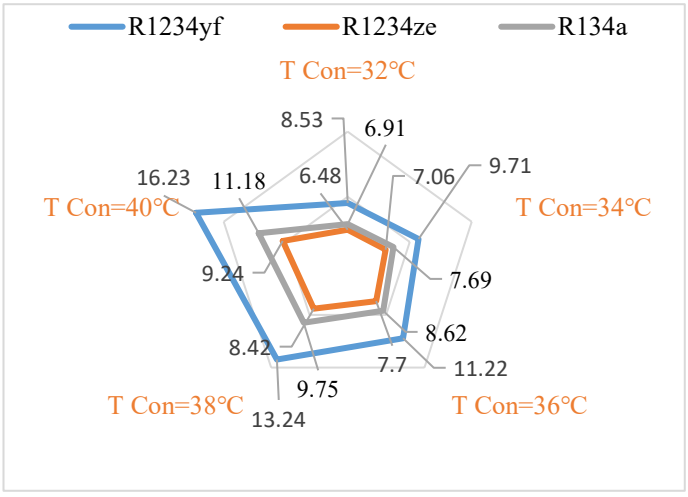

(b) Nozzle exit diameter (mm)

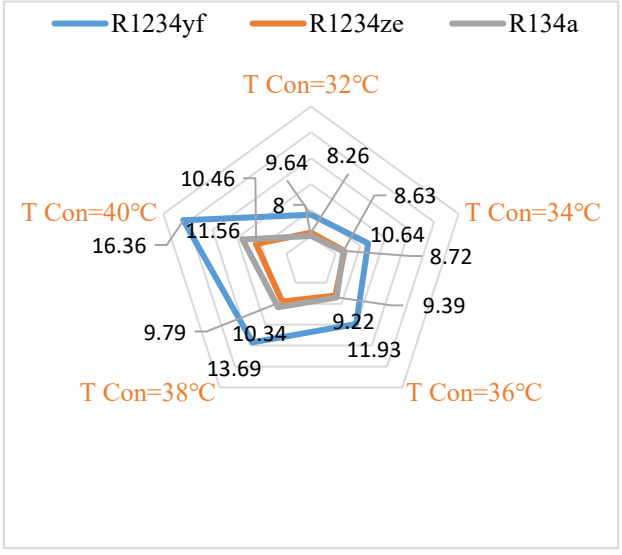

(c) Constant area diameter (mm)

Fig. 12: Influence of condenser temperature on ejector dimensions

4.2.3 On mass flow rate and heat load

Figure 13 shows that both primary and secondary mass flow rates are decreased with the decrease of condenser temperature from 40°C to 32°C. Primary mass flow is decreased more than the secondary mass flow rate, therefore the COP and μ are increased. The primary mass flow is increased more when using R1234yf as working fluid by 73.59% compared to other working fluids. The primary fluid flow rate is increased by 53.37% and 64.11% with R1234ze and R134a respectively. The requirement of primary mass is less when using R1234ze in comparison to other working fluids at any condenser temperature. The secondary mass flow rate is increased by 9.3%, 8.1%, and 5.97% when using R1234yf, R1234ze, and R134a respectively as working fluids with the decrease in condenser temperature.

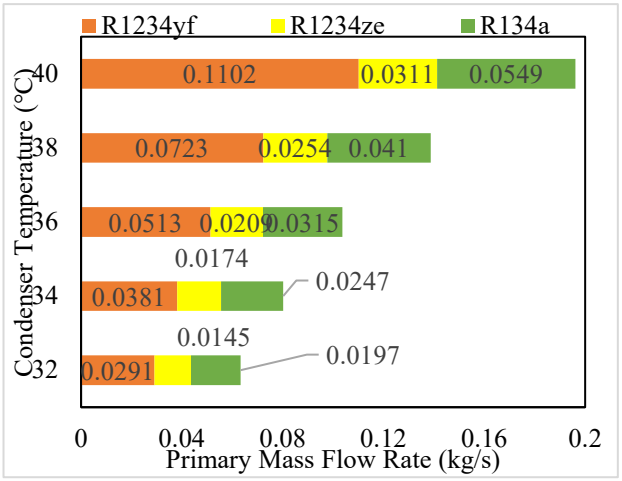

(a) Primary mass flow rate (kg/s)

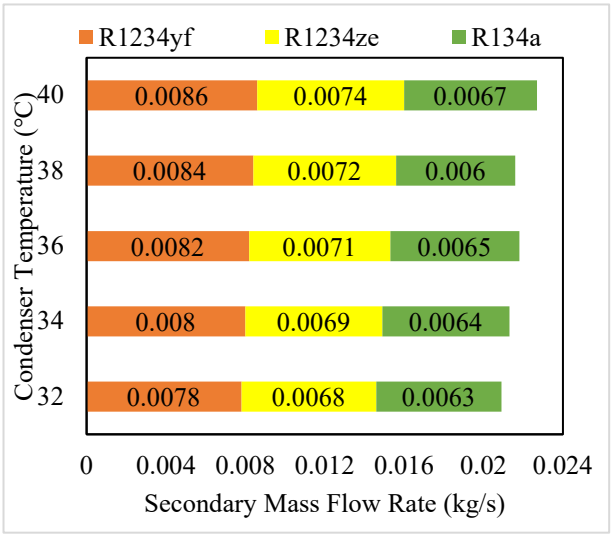

(b) Secondary mass flow rate (kg/s)

Fig. 13. Influence of condenser temperature on mass flow rate.

Figures 14 (a) and (b) show the effects of condenser temperature on the change of heat load in the generator and the condenser for the refrigerant R134a. Similarly figures 15 and 16 show variations of the same variables for the refrigerants R1234yf and R1234ze respectively. It

can be seen from the respective figures that the heat load in both the generator and condenser is increased with the increase in condenser temperature from 32°C to 40°C for the working fluid. The heat load in the generator and condenser are increased by 206.72% and 251.12% respectively when the condenser temperature is increased from 32°C to 40°C while operating at 1 kW cooling capacity with R1234yf. The heat content required in the generator is found to increase by 250% when the refrigeration capacity is increased from 1 kW to 3.5 kW. Observations are similar with R134a and R1234ze.

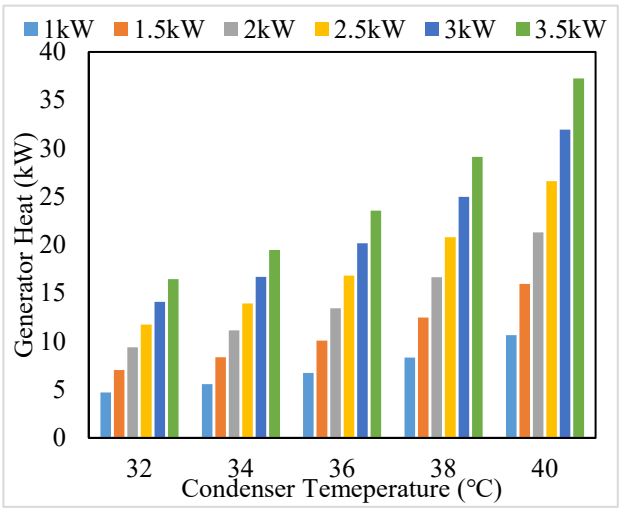

(a) Generator heat load (kW)

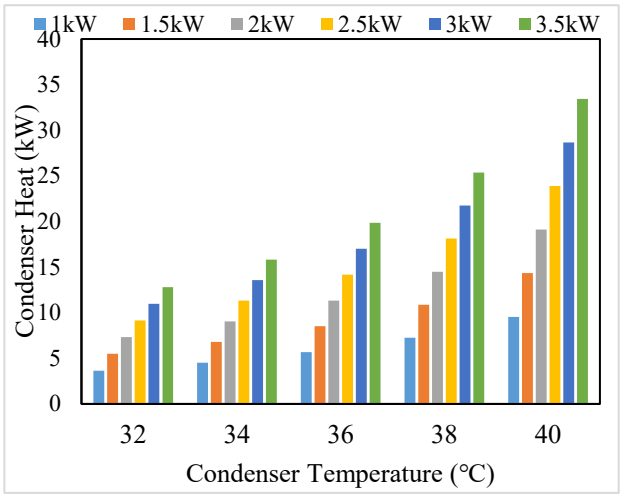

(b) Condenser heat load (kW)

Fig. 14: Influence of condenser temperature on heat load for R134a.

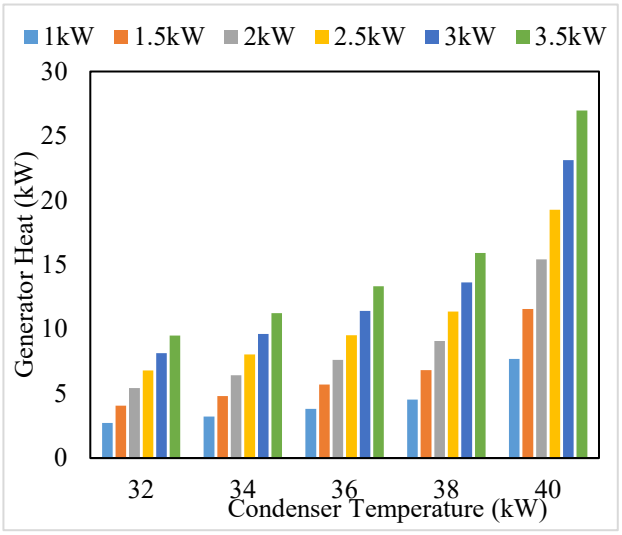

(a) Generator heat load (kW)

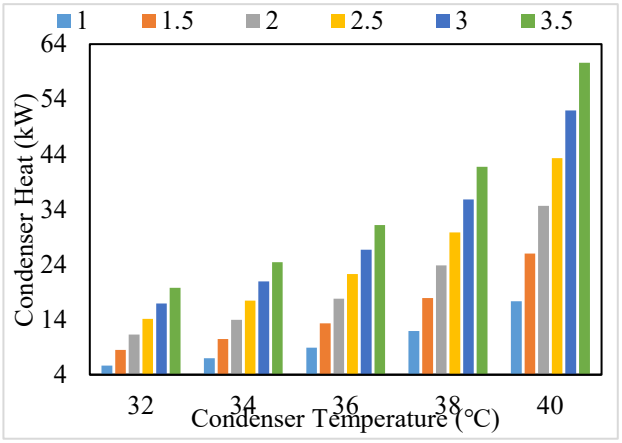

(b) Condenser heat load (kW)

Fig. 15: Influence of condenser temperature on heat load for R1234yf

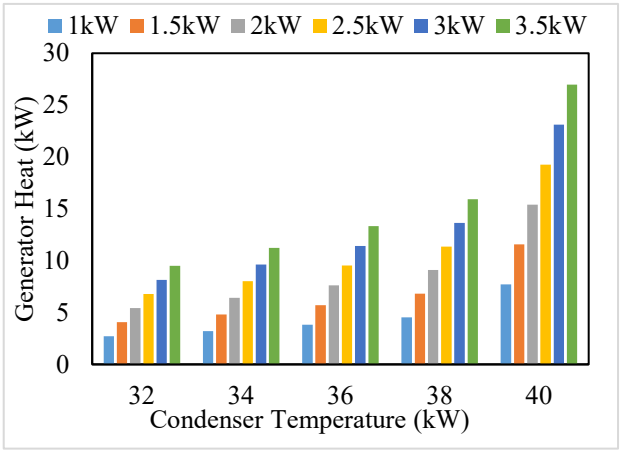

(a) Generator heat load (kW)

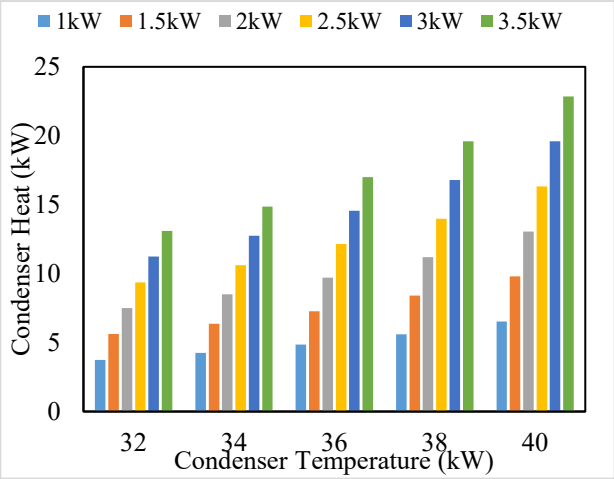

(b) Condenser heat load (kW)

Fig. 16: Influence of condenser temperature on heat load for R1234ze

4.3 Effect of superheating in the generator

4.3.1 on System performance

The degree of superheat in the generator has been varied from 2-6°C in the study. Figure 17 reveals that the performance of the system is increased with the rise in the degree of superheat in the generator. Maximum COP is 0.193 at 6 degree of superheat for R1234ze. Increasing the degree of superheat from 2 to 6°C, the maximum variation in COP is obtained for R1234yf followed by R1234ze. The trend of the entainment ratio variation is same as that of COP. However, the rate of entrainment ratio rise is maximum for R1234yf and minimum for R134a.

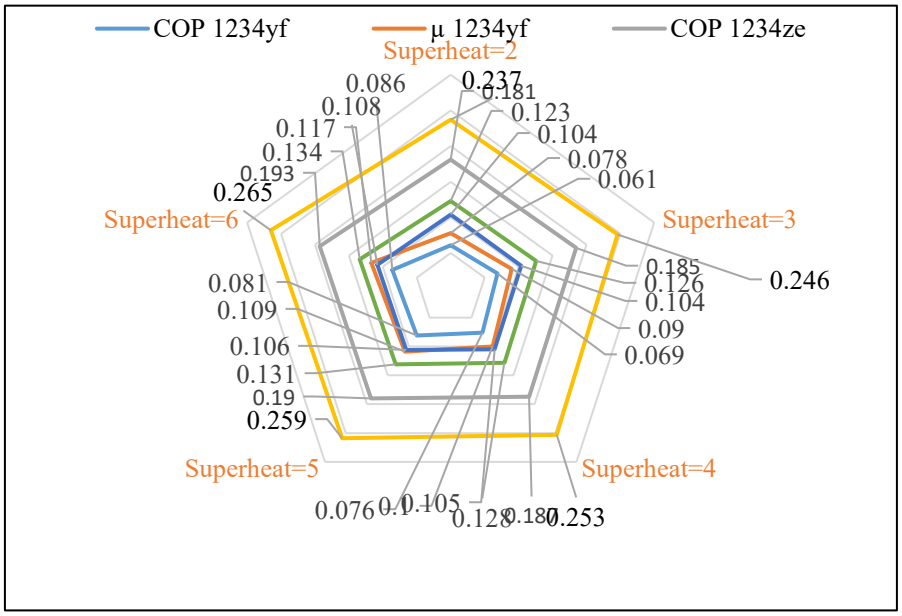

Fig. 17: Influence of degree of superheat on COP and μ

Figure 18 shows the variation of mixing pressure with the degree of superheat in generator. The mixing pressure is found to increase by the increase in superheat by 6.9%, 4.32%, and 1.96% for the R1234yf, R1234ze, and R134a respectively.

Table 4 depicts the effects on mixing area ratio and nozzle area ratio at the designed evaporator and condenser temperatures while varying the degree of superheat in the generator. The mixing area ratio of the ejector is increased by 0.53%, 0.372%, and 0.53% for R1234yf, R1234ze, and R134a working fluids respectively with the increase in degree of superheat. However, the nozzle area ratio is decreased by 3.7%, 2.4%, and 1.13% for R1234yf, R1234ze, and R134a respectively.

Table 4: Influence of degree of superheat on area ratio with different working fluids.

Super heat	R1234yf		R1234ze		R134a	
	AR Mix	AR Nozzle	AR Mix	AR Nozzle	AR Mix	AR Nozzle
2	3.77	3.71	5.30	4.14	3.78	3.55
3	3.77	3.66	5.30	4.11	3.79	3.54
4	3.78	3.63	5.31	4.08	3.79	3.53
5	3.78	3.60	5.31	4.06	3.80	3.52
6	3.79	3.57	5.32	4.04	3.80	3.51

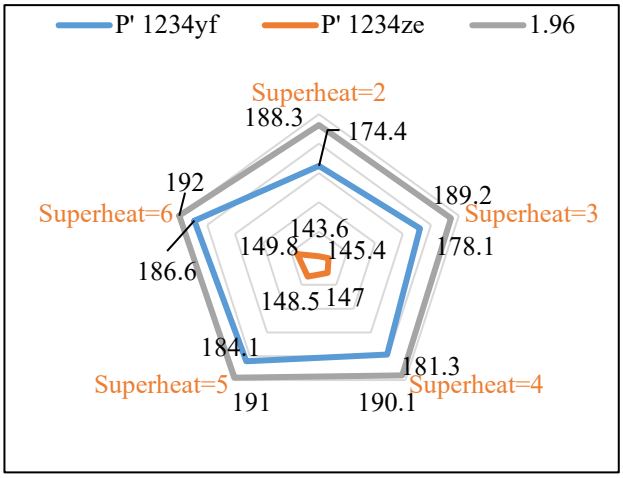

Fig. 18: Mixing pressure Influence by the variation of degree of superheat.

4.3.2 Ejector dimensions

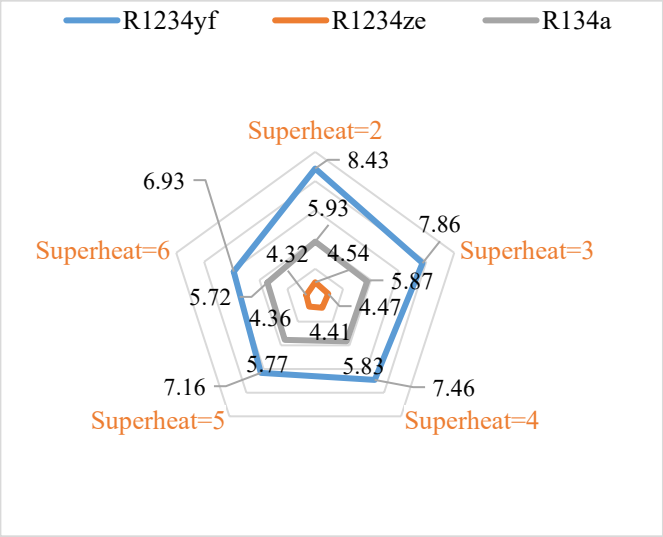

(a) Throat diameter (mm)

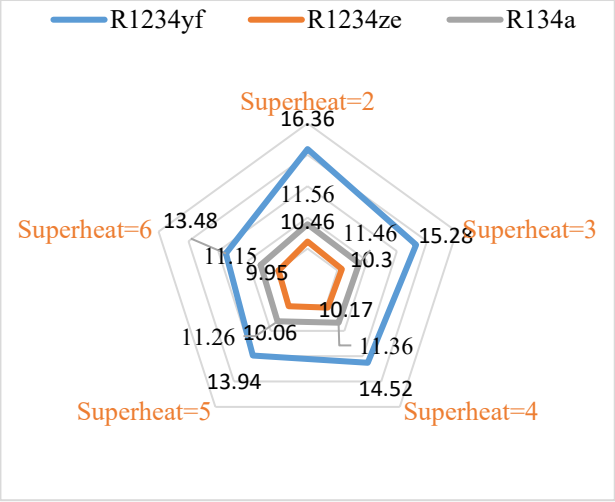

(b) Nozzle exit diameter (mm)

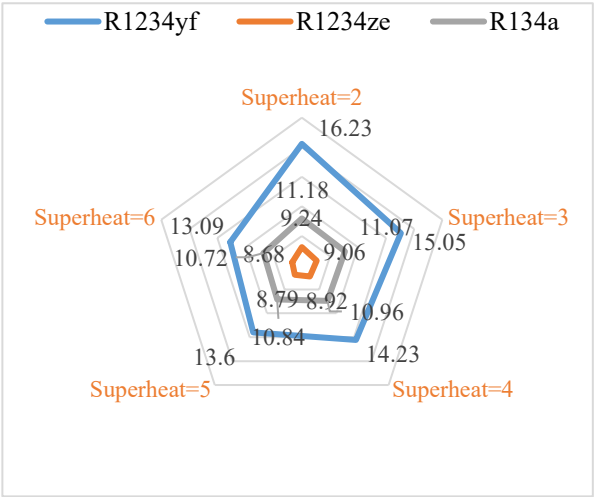

(c) Constant area diameter (mm)

Fig. 19: Influence of degree of superheat on ejector dimensions

The dimensions of the ejector also get affected by the variation of degree of superheat. Figure 19(a) shows that the throat diameter is decreased when the degree of superheat is increased. The throat diameter is found to increase by 17.79%, 4.85%, and 3.54% for R1234yf, R1234ze, and R134a respectively. The maximum throat diameter is 8.43mm for R1234yf at the degree of superheat 2, and the minimum diameter is 4.32mm for R1234ze fluid at 6 degree of superheat. The increase in degree of superheat increases the primary mass flow rate and hence improves the system performance. The effect is similar on the nozzle exit diameter with the change in degree of superheat. Figure 19(b) reveals that the nozzle exit diameter is decreased by 19.35%, 6.06%, and 4.14% for R1234yf, R1234ze, and R134a for the change in degree of superheat from 2 to 6. The maximum nozzle exit diameter is 16.23mm at 2 degree of superheat and minimum nozzle exit diameter is 8.68mm at 6 degree of superheat for R1234ze. The effect of degree of superheat on the constant area diameter also followed the same trend as the other diameters. Figure 19(c) shows that the constant area diameter is decreased with the increase of degree of superheat by 17.6%, 4.87%, and 3.55% for R1234yf, R1234ze, and R134a respectively. The constant-area diameter is always highest for R1234yf and lowest for R1234ze for the range of degree of superheat considered.

4.2.3 On mass flow rate and heat load

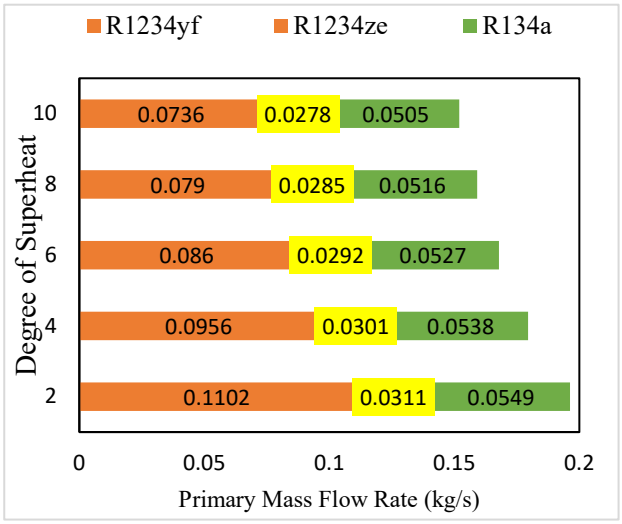

(a) Primary mass flow rate (kg/s)

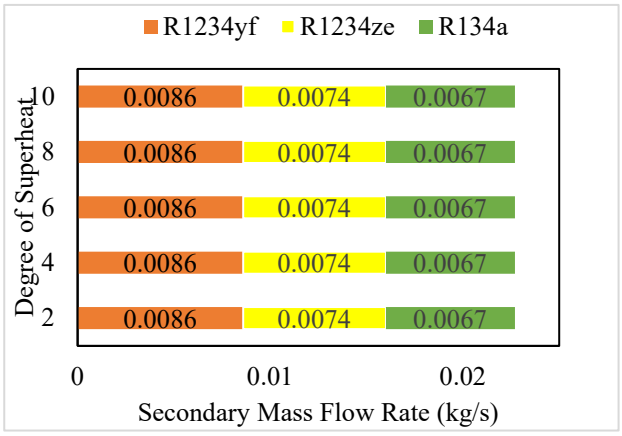

(b) Secondary mass flow rate (kg/s)

Fig. 20: Influence of degree of superheat on mass flow rate

Figure 20 represents the impact of degree of superheat on mass flow rate in the ECC. The primary mass flow is decreased more than the secondary mass flow rate, therefore the COP and μ are increased. The primary mass flow rate is decreased by 33.21% for R1234yf, 10.71% for R1234ze, 8.71% for R134a. The requirement of primary mass is less when using R1234ze in comparison to the other working fluids at any degree of superheat. The secondary mass flow rate is almost constant as 0.0086, 0.0074, and 0.0067 when using R1234yf, R1234ze, and R134a as working fluid at any degree of superheat.

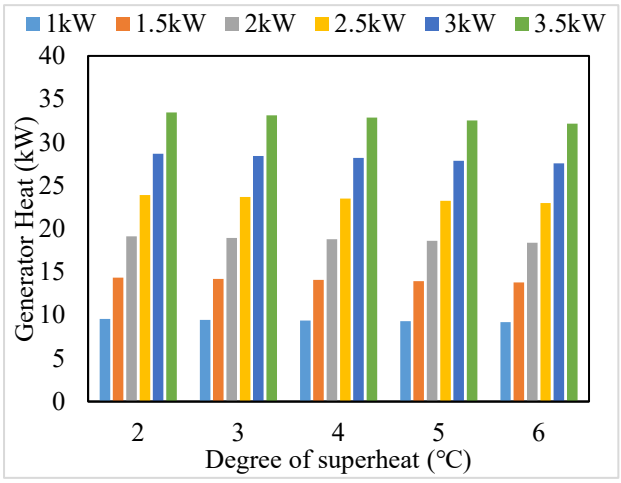

(a) Generator heat load (kW)

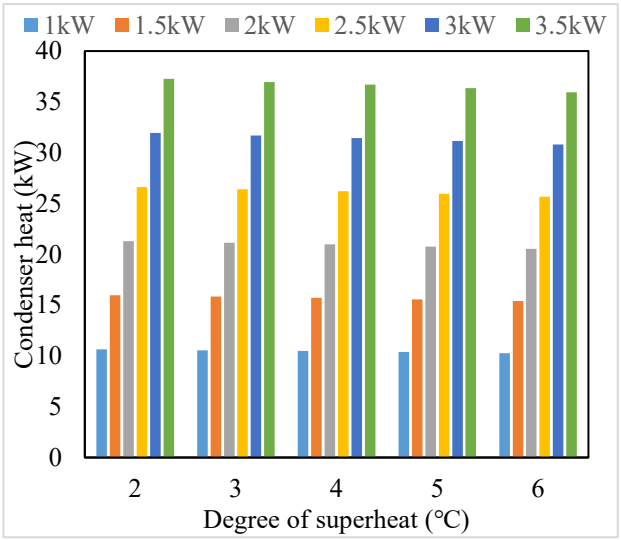

(b) Condenser heat load (kW)

Fig. 21: Influence of degree of superheat on heat load for R134a.

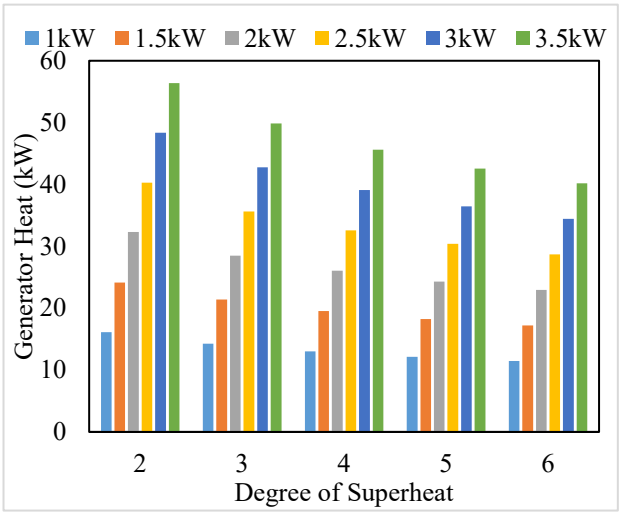

(a) Generator heat load (kW)

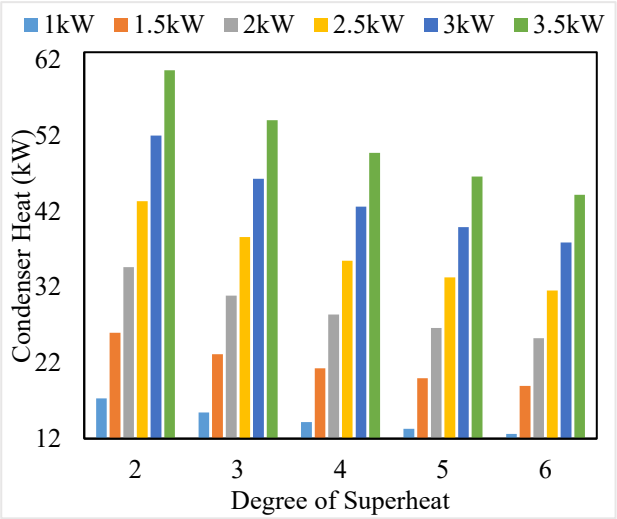

(b) Condenser heat load (kW)

Fig. 22: Influence of degree of superheat on heat load for R1234yf.

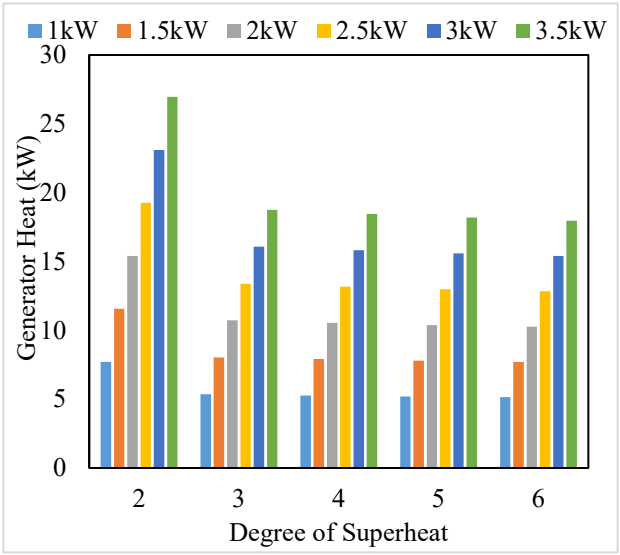

(a) Generator heat load (kW)

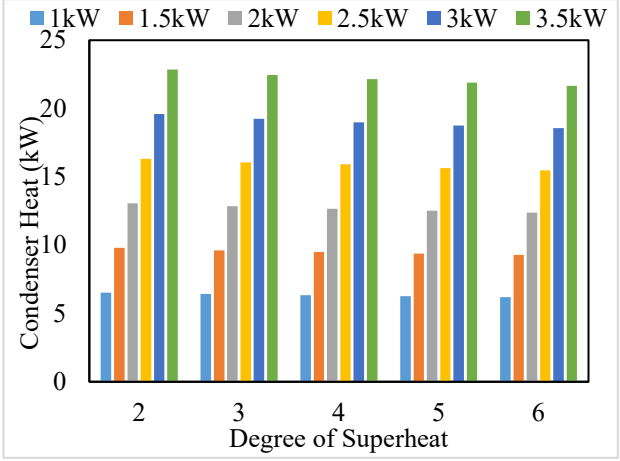

(b) Condenser heat load (kW)

Fig. 23: Influence of degree of superheat on heat load for R1234ze.

Figure 21 show the effects of degree of superheat on the change of heat load in generator and condenser for the refrigerant R134a. Similarly figures 22 and 23 show variation of the same variables for the refrigerants R1234yf and R1234ze respectively. It can be seen from the respective figures that the heat load in both generator and condenser is increased with the decrease in degree of superheat from 2 to 6 for the working fluid. The heat load in the generator and condenser are decreased by 28.72% and 27.12% respectively when the degree of superheat is increased from to 2 to 6 while operating at 1 kW cooling capacity with R1234yf. The heat content required in the generator is found to increase by 250% when the refirgeration capacity is increased from 1 kW to 3.5 kW. Observations are similar with R134a and R1234ze.

5. Conclusions:

This paper presents the performance and dimentions of ejector for a relatively new ecofriendly refrigerant R1234ze, R1234yf and is compared with R134a.

- The COP of the system at the designed condition is 0.061 (R1234yf), 0.181 (R1234ze) and 0.104 (R134a).
- The system performance is increased by 35.55% (R1234yf), 41.41% (R1234ze) and 38.67% (R134a) with the increase of evaporator temperature from 2°C to 10°C.
- The entrainment ratio of system is decreased by 71.01% (R1234yf), 49.47% (R1234ze) and 61.19% (R134a) with the change in condenser temperature from 32°C to 40°C.
- As the temperatures of generator and evaporator are increased, the nozzle's throat area is decreased; however, it is increased with the increase in condenser temeprture.
- As evaporator temperature is increased, the generator and condenser heat load are found to decrease by 34.37% and 32.37% for R1234yf, 40.93% and 34.67% for R1234ze and 38.84% and 35.21% for R134a respectively.
- The generator and condenser heat load are increased by 55.91% and 61.69% for R134a, 67.39% and 40.52% for R1234yf and 42.63% and 64.75% for R1234ze respectively with increase of condenser temperature.

Nomenclature

ALT	Atmospheric lifetime (-)
AR	Area ratio (-)
CAS	Constant area section (-)
COP	Coefficient of performance (–)
ECC	Ejector cooling cycle (-)
EES	Engineering equation solver (-)
ER	Entrainment ratio (-)
GWP	Global warming potential (-)

h	Specific enthalpy (kJ/kg)
ṁ	mass flow rate (kg/s)
M	Mach Number (-)
NXP	Nozzle exit position (-)
ODP	Ozone depletion potential (-)
P	Pressuere (kPa)
Q	Heat (kW)
V	Velocity (m/s)
W	work (kW)

Greek symbols

μ	Entrainment ratio (-)
η	Effiency (%)
θ	convergent angle (°)
γ	specific heat ratio (-)

Subscripts

Con	Condenser
d	Diffuser
Eje	Ejector
Eva	Evaporator
Gen	Generator
in	Inlet
m	Mixing
mix	Mixing section
n	Nozzle
out	Outlet
Pump	Pump
TH	Throat
TV	Throttling Valve
1,2,3..	State points
a,b,c,d	State points inside the ejector

References

1) L. Pérez-Lombard, J. Ortiz, and C. Pout, "A review on buildings energy consumption information," *Energy Build*, **40** (*3*) 394–398 (2008). doi:10.1016/J.ENBUILD.2007.03.007.
2) K.R. Ullah, R. Saidur, H.W. Ping, R.K. Akikur, and N.H. Shuvo, "A review of solar thermal refrigeration and cooling methods," *Renewable and Sustainable Energy Reviews*, **24** 499–513 (2013). doi:10.1016/J.RSER.2013.03.024.
3) I. Sarbu, and C. Sebarchievici, "Review of solar refrigeration and cooling systems," *Energy Build*, **67** 286–297 (2013). doi:10.1016/J.ENBUILD.2013.08.022.
4) J.M. Calm, "The next generation of refrigerants – historical review, considerations, and outlook," *International Journal of Refrigeration*, **31** (*7*) 1123–1133 (2008). doi:10.1016/J.IJREFRIG.2008.01.013.
5) I. Sarbu, "A review on substitution strategy of non-ecological refrigerants from vapour compression-based refrigeration, air-conditioning and heat pump systems," *International Journal of Refrigeration*, **46** 123–141 (2014). doi:10.1016/J.IJREFRIG.2014.04.023.
6) S. He, Y. Li, and R.Z. Wang, "Progress of mathematical modeling on ejectors," *Renewable and Sustainable Energy Reviews*, **13** (*8*) 1760–1780 (2009). doi:10.1016/J.RSER.2008.09.032.
7) B.J. H Keenan, E.P. Neumann, and F. Lustwerk, "An Investigation of Ejector Design by Analysis and Experiment," 1950. http://asmedigitalcollection.asme.org/appliedmechanics/article-pdf/17/3/299/6746651/299_1.pdf.
8) J.T. Munday, and D.F. Bagster', "A New Ejector Theory Applied to Steam Jet Refrigeration," n.d.
9) B.J. Huang, J.M. Chang, C.P. Wang, and V.A. Petrenko, "A 1-d analysis of ejector performance," *International Journal of Refrigeration*, **22** (*5*) 354–364 (1999). doi:10.1016/S0140-7007(99)00004-3.
10) M. Purjam, K. Thu, and T. Miyazaki, "Thermodynamic feasibility evaluation of a novel low-temperature ejector-based trans-critical r744 refrigeration cycle," *Evergreen*, **8**(*1*) 204–212 (2021). https://doi.org/10.5109/4372280.
11) M. Ouzzane, and Z. Aidoun, "Model development and numerical procedure for detailed ejector analysis and design," *Appl Therm Eng*, **23** (*18*) 2337–2351 (2003). doi:10.1016/S1359-4311(03)00208-4.
12) H. El-Dessouky, H. Ettouney, I. Alatiqi, and G. Al-Nuwaibit, "Evaluation of steam jet ejectors," 2002. www.elsevier.com/locate/cep.
13) E. Rusly, L. Aye, W.W.S. Charters, and A. Ooi, "CFD analysis of ejector in a combined ejector cooling system," *International Journal of Refrigeration*, **28** (*7*) 1092–1101 (2005). doi:10.1016/J.IJREFRIG.2005.02.005.
14) G. Sachdeva, and B. Sharma, "Exergy analysis of an ejector cooling system by modified gouy-stodola equation," International Journal of Air-Conditioning and Refrigeration, 29 (3) (2021). doi:10.1142/S2010132521500279.
15) B. Sharma, G. Sachdeva, and V. Kumar, "Exergy analysis of heat assisted ejector refrigeration system using r1234yf," IOP Conf Ser Mater Sci Eng, 1104 (1) 012035 (2021). doi:10.1088/1757-899x/1104/1/012035.
16) Dhiman, A., & Sachdeva, G. (2022). Energy and Exergy Analysis of a Pressurized Solar Cooking System Based on a Parabolic Dish Collector. Evergreen, 9(4) 1168-1180 (2022). https://doi.org/10.5109/6625728.
17) Sachdeva, G., Sharma, B., Anuradha, P., & Verma, S. (2023). Irreversibility Analysis of an Ejector Refrigeration Cycle by Modified Gouy-Stodola Formulation. Evergreen, 10(1) 252-271 (2023).

https://doi.org/10.5109/6781075
18) Alhamid, M. I., Nasruddin, N., Budihardjo, Susanto, E., Vickary, T. F., & Arif Budiyanto, M. (2019). Refrigeration cycle exergy-based analysis of hydrocarbon (R600a) refrigerant for optimization of household refrigerator. Evergreen, 6(1) 71–77 (2019). https://doi.org/10.5109/2321015
19) S. He, Y. Li, and R.Z. Wang, "A new approach to performance analysis of ejector refrigeration system using grey system theory," *Appl Therm Eng*, **29** (*8–9*) 1592–1597 (2009). doi:10.1016/J.APPLTHERMALENG.2008.07.016.
20) V. Van Nguyen, S. Varga, J. Soares, V. Dvorak, and A.C. Oliveira, "Applying a variable geometry ejector in a solar ejector refrigeration system," *International Journal of Refrigeration*, **113** 187–195 (2020). doi:10.1016/j.ijrefrig.2020.01.018. https://doi.org/10.1016/j.energy.2018.08.017
21) Y. Zhu, W. Cai, C. Wen, and Y. Li, "Numerical investigation of geometry parameters for design of high performance ejectors," *Appl Therm Eng*, **29** (*5–6*) 898–905 (2009). doi:10.1016/J.APPLTHERMALENG.2008.04.025.
22) J. Yan, W. Cai, and Y. Li, "Geometry parameters effect for air-cooled ejector cooling systems with r134a refrigerant," *Renew Energy*, **46** 155–163 (2012). doi:10.1016/J.RENENE.2012.03.031.
23) P. Haghparast, M. V. Sorin, and H. Nesreddine, "The impact of internal ejector working characteristics and geometry on the performance of a refrigeration cycle," *Energy*, **162** 728–743 (2018). doi:10.1016/j.energy.2018.08.017.
24) D.W. Sun, and I.W. Eames, "Performance characteristics of hcfc-123 ejector refrigeration cycles," *Int J Energy Res*, **20** (*10*) 871–885 (1996).
25) R. Yapici, H.K. Ersoy, A. Aktoprakoğlu, H.S. Halkaci, and O. Yiğit,"Experimental determination of the optimum performance of ejector refrigeration system depending on ejector area ratio," International Journal of Refrigeration, 31 (7) 1183–1189 (2008). doi:10.1016/J.IJREFRIG.2008.02.010.
26) Y. Jia, and C. Wenjian, "Area ratio effects to the performance of air-cooled ejector refrigeration cycle with r134a refrigerant," *Energy Convers Manag*, **53** (*1*) 240–246 (2012). doi:10.1016/J.ENCONMAN.2011.09.002.
27) S. Varga, A.C. Oliveira, and B. Diaconu, "Influence of geometrical factors on steam ejector performance – a numerical assessment," *International Journal of Refrigeration*, **32** (*7*) 1694–1701 (2009). doi:10.1016/J.IJREFRIG.2009.05.009.
28) D.T. Chong, J.J. Yan, G.S. Wu, and J.P. Liu, "Structural optimization and experimental investigation of supersonic ejectors for boosting low pressure natural gas," *Appl Therm Eng*, **29** (*14–15*) 2799–2807 (2009). doi:10.1016/J.APPLTHERMALENG.2009.01.014.
29) H. Wu, Z. Liu, B. Han, and Y. Li, "Numerical investigation of the influences of mixing chamber geometries on steam ejector performance," *Desalination*, **353** 15–20 (2014). doi:10.1016/J.DESAL.2014.09.002.
30) K. Banasiak, A. Hafner, and T. Andresen, "Experimental and numerical investigation of the influence of the two-phase ejector geometry on the performance of the r744 heat pump," *International Journal of Refrigeration*, **35** (*6*) 1617–1625 (2012). doi:10.1016/J.IJREFRIG.2012.04.012.
31) J. Chen, H. Havtun, and B. Palm, "Investigation of ejectors in refrigeration system: optimum performance evaluation and ejector area ratios perspectives," *Appl Therm Eng*, **64** (*1–2*) 182–191 (2014). doi:10.1016/J.APPLTHERMALENG.2013.12.034.
32) Klein SA (2020) EES-Engineering Equation Solver. Academic professional V10.836-3D. F-chart software, INDIA. www.fChart. com
33) W. Pridasawas, and Kungliga tekniska högskolan. Institutionen för energiteknik., "Solar-driven refrigeration systems with focus on the ejector cycle," Department of Energy Technology, Royal Institute of Technology, 2006.
34) D.W. Sun, and I.W. Eames, "Performance characteristics of hcfc-123 ejector refrigeration cycles," *Int J Energy Res*, **20** (*10*) 871–885 (1996). doi:10.1002/(SICI)1099-114X(199610)20:10<871::AID-ER201>3.0.CO;2-4.
35) J. Yu, Y. Ren, H. Chen, and Y. Li, "Applying mechanical subcooling to ejector refrigeration cycle for improving the coefficient of performance," *Energy Convers Manag*, **48** (*4*) 1193–1199 (2007). doi:10.1016/j.enconman.2006.10.009.
36) J. Yu, and Y. Li, "A theoretical study of a novel regenerative ejector refrigeration cycle," *International Journal of Refrigeration*, **30** (*3*) 464–470 (2007). doi:10.1016/J.IJREFRIG.2006.08.011.
37) D.-W. Sun, "Performance Characteristics Of Hcfc-123 Ejector Refrigeration Cycles," 1996.
38) B. Saleh, "Performance analysis and working fluid selection for ejector refrigeration cycle," *Appl Therm Eng*, **107** 114–124 (2016). doi:10.1016/j.applthermaleng.2016.06.147.